Soft Matter

PAPER

View Article Online
View Journal | View Issue

Check for updates

Cite this: *Soft Matter*, 2020, **16**, 8002

Patchy rough colloids as Pickering stabilizers†

Hannah M. H. Weijgertze, Willem K. Kegel* and Michele Zanini *

Pickering stabilizers are typically considered to be perfectly smooth and chemically homogeneous. The use of rough and heterogeneous colloids is expected to fundamentally alter the properties of emulsions. In particular, we investigate the role of surface structuring in the emulsification and catastrophic phase inversion of Pickering emulsions. To gain deeper fundamental insights into this topic, we fabricate in a controlled and simple manner patchy rough particles with a polystyrene core and organosilicate asperities. As a consequence of the synthesis, the surface roughness and chemical heterogeneity are coupled, namely the chemical heterogeneity is directly connected with the surface patchiness. The synthesis is robust, scalable and leads to the production of grams in less than a day. The geometrical roughness is characterized with AFM, while the chemical composition is extracted from oxidative mass loss upon combustion. Wetting studies are empirically carried out using a gel trapping technique and the results are compared with the theoretically derived contact angles of particles. Systematic variations in the emulsification shear rate, oil/water ratio and particle type reveal the influence of particle heterogeneity on the formation and formulation of emulsions. This work paves the way for a deeper understanding of the behavior of Pickering emulsions, where non-ideal, heterogeneous particles are present.

Received 5th May 2020,
Accepted 16th July 2020

DOI: 10.1039/d0sm00807a

rsc.li/soft-matter-journal

Open Access Article. Published on 18 July 2020. Downloaded on 4/5/2026 3:19:30 AM.
This article is licensed under a Creative Commons Attribution-NonCommercial 3.0 Unported Licence.

Introduction

Emulsions are widely spread in many different fields of our daily life, such as in food,[1] cosmetics,[2] paints,[3] pharmaceutical products[4,5] and petroleum industries.[6] Conventionally, an emulsion is a mixture of two immiscible liquids, where one phase is dispersed (the dispersed phase) into the other (the continuous phase).[7] Surface active species stabilize the droplets and prevent emulsions from phase separation. Traditionally, surfactant molecules are used as emulsion stabilizers.[8]

Since the pioneering work of Ramsden[9] and Pickering,[10] the potential of solid particles to stabilize emulsions has been recognized and exploited. Pickering emulsions can offer advantages over surfactant-stabilized emulsions, namely increasing the emulsion stability, providing more environmentally friendly processes and reducing the use of potentially toxic or irritant chemical mixtures.[11] In general, (Pickering) emulsions are a flexible material platform, where either oil-in-water (o/w) or water-in-oil (w/o) emulsion types can be accessed depending on emulsification conditions and processing.[12,13] In a Pickering emulsion, layers of solid particles on droplets create a steric barrier against coalescence and disproportionation.[14] The position of the particles at the interface, given by the contact angle θ, is dictated by the wettability. Conventionally, the contact angle of particles at an oil–water interface is measured through the water phase. Hydrophilic particles are mostly immersed in the aqueous phase and thus have a contact angle $\theta < 90^\circ$. According to the Bancroft rule, they preferentially stabilize oil droplets (o/w). Conversely, hydrophobic particles have contact angles $\theta > 90^\circ$ and usually stabilize w/o emulsions.

Interestingly, Pickering stabilizers are typically considered smooth and chemically homogeneous spheres.[5,15] However, the particles present in real systems often do not fulfill these requirements. For instance, clay,[16,17] protein[11,18] and starch[19,20] particles have been extensively used as emulsion stabilizers, especially in the food industry,[20] despite the fact that they bear a wide variety of morphologies and have chemically heterogeneous compositions.

Designing particles with a broad diversity of morphologies as Pickering stabilizers has gained interest in recent years. Such particles include Janus particles,[21] (Janus) sheets,[22,23] ellipsoids,[24] dumbbells[25] and rough particles.[26–28] Remarkably, particle shapes deviating from homogeneous spheres affect emulsification and give opportunities for different Pickering stabilization.[5,29–32] For Janus particles, the combination of patch size and wetting contrast has been proved to affect the nature of emulsions. In particular, this is true when the wetting contrast between lobes is significant. Otherwise, the patch size plays a negligible role in emulsification.[32]

Van't Hoff Laboratory for Physical and Colloid Chemistry, Debye Institute for Nanomaterials Science, Utrecht University, Utrecht, The Netherlands.
E-mail: michele.zanini.mfz@gmail.com, W.K.Kegel@uu.nl

† Electronic supplementary information (ESI) available: Synthesis and characterization of patchy rough colloids. Additionally, the ESI reports the methodology adopted for the emulsification and the image analysis used to characterize the emulsion type. See DOI: 10.1039/d0sm00807a

This journal is © The Royal Society of Chemistry 2020

Open Access Article. Published on 18 July 2020. Downloaded on 4/5/2026 3:19:30 AM.
This article is licensed under a Creative Commons Attribution-NonCommercial 3.0 Unported Licence.

In this work, the use of well-characterized patchy rough particles as Pickering stabilizers is investigated to better understand the effect of particle heterogeneity on emulsification. In particular, we focused on the role of surface structuring in the phase inversion of emulsions. Phase inversion concerns the switch from an o/w to a w/o emulsion or *vice versa*.[12] It can be catastrophic or transitional. The former is obtained by varying the w/o ratio,[33] whereas the latter by tuning the particle contact angle.[34]

A considerable body of work has been dedicated to trigger transitional phase inversion. Successful strategies comprise not only the variations of temperature,[35] surfactant concentration,[36,37] pH and ionic strength,[14,38–40] but also the use of peculiar *ex situ* drying processes[41,42] or different apolar phases.[43] Emulsion phase inversion is relevant to many industrial processes, including the fabrication of cosmetics, food and pharmaceutical products, as well as crude oil recovery.[6,44] Interestingly, in cosmetics[45] and food science,[46] phase inversion is typically undesired since it completely alters the product properties. More interestingly, in crude oil processing, phase inversion is deployed to recover oil from emulsions.[47] The opposite use of emulsion phase inversion reported in different industries underlines the crucial importance of controlling its onset.

To achieve our goal, both the o/w ratio and energy input during emulsification are systematically varied to gain more insights into the effect of surface heterogeneity on the emulsification and phase inversion of Pickering emulsions. In this regard, patchy rough particles comprising a polystyrene core with organosilicate asperities are fabricated in large quantities. The synthetic path is based on wet chemistry and has been proved to be scalable. In fact, several grams of colloids can be reproducibly fabricated in two subsequent steps without the need of any intermediate purification. The synthesis takes inspiration from the heteronucleation of liquid organosilicates under alkaline conditions on hydrophobic colloids.[48–50] We applied atomic force microscopy (AFM) and thermogravimetric analysis (TGA) to characterize the roughness of the products and to obtain the degree of chemical heterogeneity, respectively. The latter is directly connected with surface patchiness and it allows the estimation of the equilibrium positions of the particles at a water–oil interface. These theoretical values differ from the contact angles empirically measured with a gel trapping technique (GTT). This evidence underlines the non-trivial adsorption pathway of the non-ideal particles at liquid interfaces and the possibility to explore kinetically stable out-of-equilibrium configurations. In all our experiments, the colloids are initially dispersed in the aqueous phase, where they are charge-stabilized. The considerations and conclusions connected to the particles at fluid interfaces reported in this manuscript are based on single-particle mechanisms. Kinetic effects associated to the bending rigidity and extra deviatoric interfacial rheology of colloidal monolayers go beyond the scope of this work.

Experimental (materials and methods)

Materials

4-Styrenesulfonic acid sodium salt hydrate (NaSS, Sigma-Aldrich), 2,2′-azobis(2-methylpropionitrile) (AIBN, 98%, Sigma-Aldrich), methanol (MeOH, absolute HPLC, Biosolve Chimie), divinylbenzene (DVB, technical grade 80%, Sigma-Aldrich), methacryloxyethyl thiocarbamoyl rhodamine B (PolyFluor®570, Polysciences), ammonium hydroxide (NH_4OH, 28–30 wt% in water, Acros Organics), 3-(trimethoxysilyl)propyl methacrylate (TPM, ≥97%, Sigma-Aldrich), dimethyl sulfoxide (DMSO, Sigma-Aldrich), gellan gum (gellan, powder, Alfa Aesar), ethanol (EtOH, absolute, VWR Chemicals), Norland optical adhesive 81 (UV glue, Norland), pyrromethene BODIPY™ 493/503 (BODIPY, Invitrogen™), potassium chloride (KCl, ≥99%, Acros Organics), *n*-decane (≥99%, Carl Roth GmbH) and hydrochloric acid (HCl, 37% in water, Acros Organics) were used as received. Styrene (≥99%, containing 4-*tert*-butylcatechol as a stabilizer, Sigma-Aldrich) was purified through a column packed with silica gel (high purity grade: Davisil Grade 633, Sigma-Aldrich) and aluminum oxide powder (≥98%, Honeywell Fluka). The water used in all experiments was purified by filtration through Millipore filters (18.2 MΩ cm at 25 °C).

Polystyrene core particle fabrication

Cross-linked sulfonated polystyrene (PS) particles were fabricated *via* dispersion polymerization.[51] For the synthesis, 5 mL styrene, 90 mg NaSS and 90 mg AIBN were dissolved in 10 mL water and 40 mL MeOH in a 100 mL round-bottom flask. Since the reaction medium is a good solvent for the monomer, the mixture was initially homogeneous.[52] The formation and precipitation of the polymer particles created a dispersion. The flask was sealed with a rubber septum and flushed with N_2 (g) for 30 minutes under magnetic stirring at 200 rpm. Next, the flask was immersed in a pre-heated oil bath (65 °C) and the mixture was stirred magnetically at 200 rpm. After 5 hours, a pre-heated (50 °C) mixture of 0.5 mL styrene, 165 μL DVB, 90 mg AIBN and 1 mg PolyFluor®570 in 5 mL MeOH was added to cross-link the polymer particles and equip them with a fluorescent label. The polymerization was continued for 24 hours. The resulting polystyrene particles were washed three times in MeOH/water by centrifugation at 3270 × *g* (Beckman Coulter Allegra® X-12R). Washing in the MeOH/water mixture rather than only in water facilitated sedimentation and redispersion of the particles. If necessary, redispersion was promoted by mechanical agitation and sonication. Rotary evaporation was used to remove MeOH. The final particle concentration of the PS core dispersions was 3.5–4.0 wt%.

Fabrication of patchy rough colloids

In order to obtain sufficient amounts of particles to extensively study their emulsification behavior, the synthesis was scaled to yield nearly a gram of patchy rough (or raspberry-like) particles per batch. To achieve this goal, heteronucleation and polymerization of the organosilicate TPM on PS cores was used.[53] To do so, a volume of 20–30 mL of the PS core dispersion was added to a 2 L Teflon bottle containing 974 mL water and 52 mL NH_4OH (pH 11.5) such that the PS particle concentration in the final reaction volume was *circa* 3×10^{12} particles per mL. TPM was added in the range of 0.17–0.32 vol% with respect to the total reaction volume to obtain different degrees of particle roughness

Open Access Article. Published on 18 July 2020. Downloaded on 4/5/2026 3:19:30 AM. This article is licensed under a Creative Commons Attribution-NonCommercial 3.0 Unported Licence.

and composition. The bottle was agitated on a tumbling table (IKA® KS 260 basic) for 90 minutes at 150 rpm. This allowed the TPM to undergo a sol–gel process[54] and to heteronucleate on PS spheres. Thereafter, the reaction mixture was transferred to a 2 L round-bottom flask and 240 mg of AIBN (initiator) was added.[55] During this step, 280 μL of 1 mg mL^{-1} BODIPY in DMSO can be added to label the asperities with a green fluorescent marker. The flask was flushed with N_2 (g) for 15 minutes and sealed before being immersed in an oil bath (80 °C). The TPM was polymerized on the PS cores under magnetic stirring at 200 rpm for 2 hours. The fabricated patchy rough particles were washed three times by centrifugation at 10 000 × *g* (Beckman Coulter Avanti J-26 XP, rotor JLA-16.250) and redispersed in water.

Scanning electron microscopy

PS particle size distributions were determined from SEM images (scanning electron microscopy, Phenom ProX). The surface topography of the fabricated patchy rough particles was visualized with SEM (XL30S FEG, FEI). The SEM samples were prepared by drying a suspension droplet on a hydrophilized Si wafer (Sil'tronix 1–20 Ω cm, P-doped; glow-discharged with a Cressington Carbon Coater 208C and Power unit 208APU). The samples were sputter-coated with a few nanometers of Pt to prevent charging (Cressington Sputter Coater 208HR). All SEM samples reported in this work were prepared in the same manner.

Zeta potential

The zeta potential measurements of ~0.03 wt% PS particle suspensions in 10 mM KCl were conducted with a Malvern Zetasizer Nano ZS in a disposable cuvette (polystyrene, 4 mL, SARSTEDT AG & Co. KG). The Smoluchowski model was applied to extract the zeta potential values.

AFM roughness characterization

The surface roughness of the produced particles was measured by scanning a particle monolayer with AFM (atomic force microscopy, JPK NanoWizard II). The AFM samples were prepared by convective assembly[56] of particles on a hydrophilized glass slide (VWR cover glass 22 × 22 mm^2, #1.5 thickness, glow-discharged with a Cressington Carbon Coater 208C and Power unit 208APU). The particle surface was probed with an Olympus AC160TS-R3 silicon cantilever with a resistivity of 0.01–0.02 Ω cm, a spring constant of 26 N m^{-1} and a resonance frequency of 300 kHz at room temperature and ambient relative humidity. The resulting AFM height profiles were analyzed to characterize the particle roughness. Since all the particles have similar size and surface topography, the RMS (root-mean-square) roughness is a suitable parameter to describe the surface topology.[27,30,57] From the AFM height profiles, the RMS roughness can be extracted using a least-squares based algorithm[27] that decouples the signal of interest from the underlying curvature. The RMS roughness can then be calculated using the following standard definition for root-mean-square deviations:

$$\text{RMS roughness} = \sqrt{\frac{1}{n}\sum_{i=1}^{n} y_i^2} \quad (1)$$

This means that the surface is sampled over n points with each having a corresponding height y_i normal to the fitted sphere. The calculated RMS was considered reliable and the extracted value was accepted when the fitted particle radius was within 10% of the average core particle radius independently determined by SEM. In this way, the diameters obtained upon fitting the AFM data coincide with the direct SEM measures presented in Fig. S9 (ESI†). This excludes tip convolution effects or scan artifacts.

Thermogravimetric analysis (TGA)

To estimate the composition of the patchy rough particles, thermogravimetric analysis was performed. For each measurement, 0.5–1.5 mL of the particle dispersion at 2–4 wt% was dried in a porcelain dish (Incinerating dishes porcelain 33d/3, IDL GmbH) in an oven. Thermogravimetric analysis was conducted using a Nabertherm P330 furnace. The samples were heated to 650 °C at a heating rate of 7 °C min^{-1} and kept for 30 min at 650 °C before being cooled down to room temperature.

The mass of different patchy rough particles before and after calcination was determined on an analytical balance. From these values, the composition of the particles expressed as the mass% of TPM could be calculated taking into account the difference in oxidative mass losses upon the combustion of PS and TPM. In Section S2 (ESI†), the calculation is explained in detail.

Surface patchiness estimation

Since the patchy rough particles are composed of PS cores with TPM asperities grown on them, the surface of the particles is chemically heterogeneous. As a quantification of the surface patchiness, the partition between PS and TPM surface areas was estimated. In this work, surface patchiness is defined as the fraction of TPM patches on the total surface. SEM images (SEM XL30S FEG, FEI) were used for the surface patchiness analysis. In particular, the average asperity size and the average number of asperities per particle were manually measured (representative images can be found in Section S3, ESI†). For a 2D estimate of the surface patchiness, the area of the TPM asperities was approximated as their projected area. Alternatively, for a 3D estimate, the TPM asperities were approximated as spherical caps with an average base radius calculated from the SEM asperity size and an average height extracted from AFM height maps.

Contact angle measurements

To study the adsorption and wetting of the fabricated particles, the particle contact angles at a water–decane interface were measured using a gel trapping technique (GTT).[58] First, a 2 wt% gellan solution in water was prepared by stirring the mixture for 2 hours at 80 °C. The gellan solution was poured into a 35 mm Petri dish containing *n*-decane inside an oven (Memmert Model 100–800) at 70 °C. Particle dispersions of 0.1–2 wt% in water/EtOH 1/1 v/v were spread at the interface by pipetting 5 μL twice on the hot gellan/water–decane interface. The addition of EtOH to the particle dispersions favors the spread of particles at the interface driven by a Marangoni flow.[59] To reliably determine contact angles with this technique, it is important that the

 This journal is © The Royal Society of Chemistry 2020

Open Access Article. Published on 18 July 2020. Downloaded on 4/5/2026 3:19:30 AM.
This article is licensed under a Creative Commons Attribution-NonCommercial 3.0 Unported Licence.

gellan addition to water does not significantly alter the adsorption of the particles at the interface. As an indication, the contact angle of a water drop under decane on hydrophobized glass is invariant to the gellan concentration in the aqueous phase.[60]

After spreading the particles, the samples were slowly cooled down to room temperature, whereby the aqueous phase jellified and the particles were immobilized at the interface. Interface replicas were obtained by replacing *n*-decane with the UV glue and curing the glue by UV illumination. In this manner, the particles are partially embedded in the UV glue, preserving their positions with respect to the interface. The replicas were imaged with SEM (Phenom ProX). Details on the calculation of the contact angles from SEM images can be found in Section S4 (ESI†).

Emulsion preparation

To investigate the effect of the use of heterogeneous particles on emulsification and phase inversion, emulsions were prepared with different o/w ratios and frothed at different shear rates.

Emulsions stabilized with patchy rough particles were produced according to the formulations given in Table 1. As references, bear PS cores and all-TPM particles were used as emulsifiers. The synthesis and characterization of all-TPM particles is described in Section S1 (ESI†). The water phase of the emulsions was prepared by adding 0.1 M KCl to 2–3 wt% particle dispersions in water to yield water phases at the weight percentages given in Table 1. BODIPY at 10^{-3} mg mL^{-1} was added in the *n*-decane oil phase to obtain sufficient optical contrast between the oil and water phases and directly visualize the formed emulsion type *via* fluorescence microscopy.

The concentration of the particles in the aqueous phase was reduced to 0.43 wt% for φ_{water} = 0.7 to ensure that the total number of colloids participating in the emulsification was constant. The pH of the emulsions was adjusted to 5.5–6.5 (monitored using a HANNA Instruments pH 210 pH meter with a Mettler Toledo InLab® Micro electrode) by adding a maximum of 120 μL of 0.2 M HCl and the respective amount of oil. Similar ionic strength and pH of the emulsions are important because the variation in these quantities may induce transitional phase inversion linked to (de)ionization of PS sulfate and TPM silanol surface groups.[61]

The emulsification was performed with an IKA® T25 digital ULTRA-TURRAX homogenizer at 8000 rpm, 14 000 rpm or 20 000 rpm for 1 minute.

Emulsion characterization

The emulsions were imaged and characterized by bright field and fluorescence microscopy within a day after their preparation.

Table 1 Emulsion formulations. In the oil phase, BODIPY was added. The aqueous phase contained 0.1 M KCl and the particles

Water fraction (φ_{water} vol. ratio)	Oil phase (mL)	Water phase (mL)	Solid load in aq. phase (wt%)
0.3	4.2	1.8	1
0.5	3	3	1
0.7	1.8	4.2	0.43

The microscopy samples were prepared by carefully pipetting the emulsion droplets in a custom-made cell consisting of two glass slides (Thermo Scientific Menzel Gläser microscope slide 76 × 26 mm^2) glued on top of each other, where a hole of 1.5 cm in diameter had been cut out. The cell was sealed with a cover glass (VWR cover slip 22 × 22 mm^2, #1.5 thick).

The obtained emulsion type (o/w or w/o) was observed with a Nikon Eclipse TE2000-U equipped with a Nikon D-Eclipse C1 laser scanning confocal microscope system. A 488 nm Ar laser was used for the excitation of the BODIPY dye in the oil phase. In the case of the co-existence of w/o and o/w, the dominating emulsion type has been estimated *via* visual inspection comparing the numbers of bright and dark pixels of several images.

Bright field images were collected with either a Nikon Eclipse Ti-E microscope with a Hamamatsu C11440 ORCA-Flash4.0 digital camera (2048 × 2044 px images) or a Nikon Eclipse Ti-U microscope with an Imaging Source DFK 33UX249 (1920 × 1200 px images).

Results and discussion

Patchy rough colloids

The dispersion polymerization of styrene and 4-styrene sulfonic acid in a water/MeOH reaction medium, yielded PS particles with diameters of ∼800 nm. The synthesis leads to monodisperse colloids and to reproducible particle sizes (Fig. S9 in Section S5, ESI†). Three batches of PS particles (PS-0, PS-I and PS-II) were produced. These particles serve as cores for the fabrication of patchy rough particles. The presence of 4-styrene sulfonic acid during the synthesis together with the sulfonated initiator ensures the surface of the PS colloids is equipped with sulfate groups. This renders the surface sufficiently negatively charged to provide colloidal stability during the synthesis of the patchy rough particles.[62] The average zeta potentials are in the range of −45 to −65 mV (see zeta potential distributions in Section S5, ESI†).

Rough particles of various morphologies can be produced by the heteronucleation and polymerization of TPM on pre-fabricated sulfonated PS particles. The formation of bumpy asperities of TPM on PS relies on the finite wetting between the two materials. The size and number of asperities formed on the PS particles depend on both the concentration of the TPM monomer and the pH set during the synthesis. Increasing the concentration of the TPM monomer results in larger lobes, while increasing the pH produces smaller and more numerous asperities (Fig. S11 in Section S6, ESI†).

To obtain patchy rough particles, the synthesis conditions were finely adjusted such that 'berry-covered' surfaces were formed. In the literature, particles with such a morphology are also commonly referred to as raspberry-like particles.[27,63] Fig. 1 schematically shows the path followed for the fabrication of patchy rough particles. In the first stage, TPM hydrolyzes and condensates *via* its silanol group[54] heteronucleating on the surface of the PS cores. The radical polymerization of the methacrylate moiety fixes the shape of the asperities and creates fully-solid raspberry-like particles. The procedure presented in

Open Access Article. Published on 18 July 2020. Downloaded on 4/5/2026 3:19:30 AM.
This article is licensed under a Creative Commons Attribution-NonCommercial 3.0 Unported Licence.

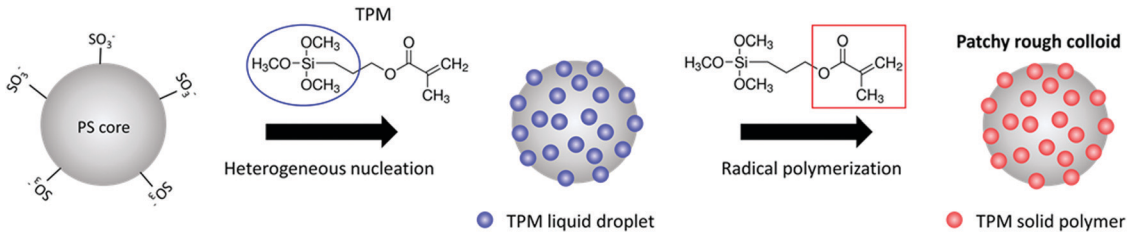

Fig. 1 Schematic of the PS/TPM patchy rough colloid synthesis.

this work reproducibly yielded up to a gram of patchy rough colloids per synthesis, which is an adequate amount to extensively study the emulsification of the particles.

Particles with different degrees of roughness and chemical composition were fabricated by varying the volume fraction of TPM at a constant pH (pH = 11.5). The size of the TPM condensate is adjusted by tuning the TPM volume fraction at a constant pH. This follows the same trend observed with the homogeneous nucleation of TPM in alkaline conditions[54] (see Section S1, ESI†). Table S1 in Section S7 (ESI†) reports the details of the synthesis and lists the fabricated particles in order of increasing roughness. Hereafter, the rough particles are referred to as 'raspberry' (RB).

Surface patchiness and contact angles

The surface topography of the fabricated patchy rough particles is imaged and characterized by both SEM and AFM, as shown in Fig. 2. The particle-by-particle root-mean-square (RMS) roughness could be extracted from the AFM height maps. The RMS roughness is a suitable parameter to compare the particle roughness since all the colloids have similar sizes and the surface morphologies are analogous. RMS roughness values of 4.1–20 nm could be achieved by varying the concentration of the TPM monomer in the reaction mixture from 0.17 to 0.32 vol%.

The RMS roughness solely describes the surface topography. Thus, a complementary characterization of the patchy rough particles focusing on their chemical composition was carried out. In this regard, thermogravimetric analysis (TGA) was used. It can be concluded that PS (almost) completely degrades upon heating the sample to 650 °C for 30 min, while 30% of the TPM mass is conserved (see Section S2, ESI†). This allows the calculation of the PS/TPM weight ratio in the patchy rough particles.

Fig. 3a presents the roughness and composition of the particles as a function of the TPM volume fraction in the reaction mixture. Both the RMS roughness and mass% TPM exhibit the same sigmoidal dependence on the vol% TPM in the reaction mixture. This denotes a strong coupling between surface heterogeneity and surface roughness and a marked dependence of the particle roughness and composition on the TPM concentration between ~0.2 vol% and ~0.3 vol%. For concentrations below or above this range, the TPM concentration has a milder impact on the particle roughness. In both cases this is connected to the spherical nature of the roughness. In general, high roughness values are obtained with a multitude of "tall" asperities. For spherical asperities, the height of the asperities determines to the largest extent the RMS, while

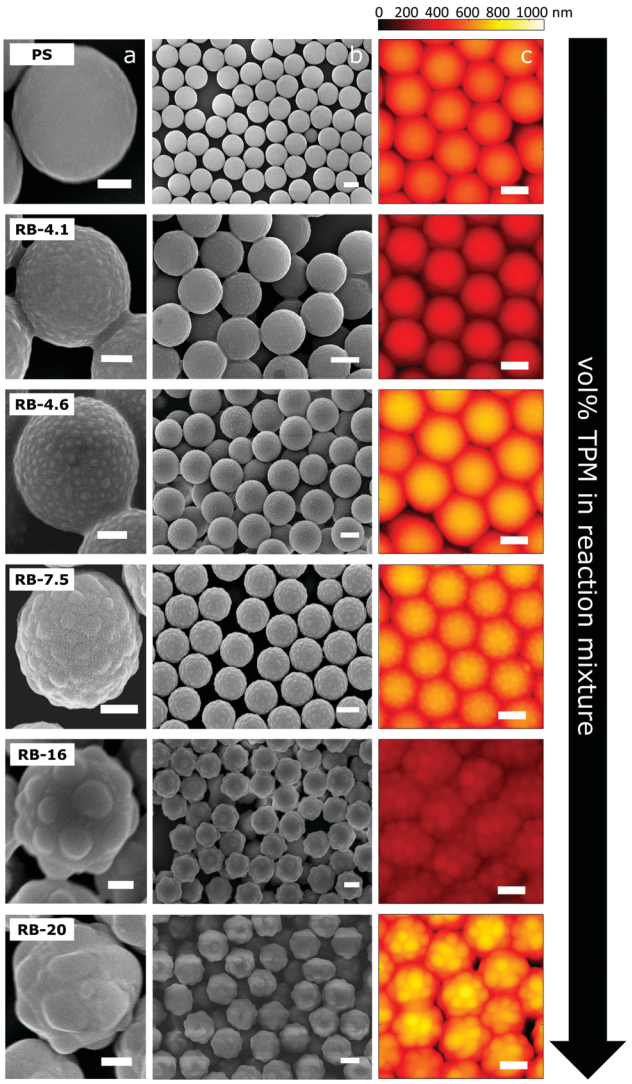

Fig. 2 Particle topography. Topographical particle surface characterization by SEM (a and b) and AFM (c). Scale bars: 200 nm (a) and 500 nm (b and c).

the asperity density has a minor influence on the RMS.[27] Additionally, for our geometry, the height and the cross-sectional diameter are coupled. Thus, an increase in height is necessarily associated with a decrease in the number of asperities per unit area. The mirrored scenario takes place for small asperities. This trade-off naturally mitigates the effect of the TPM vol% on the roughness of patchy rough colloids at the extremes of the synthesis regime. A detailed analysis of the

This journal is © The Royal Society of Chemistry 2020

Open Access Article. Published on 18 July 2020. Downloaded on 4/5/2026 3:19:30 AM.
This article is licensed under a Creative Commons Attribution-NonCommercial 3.0 Unported Licence.

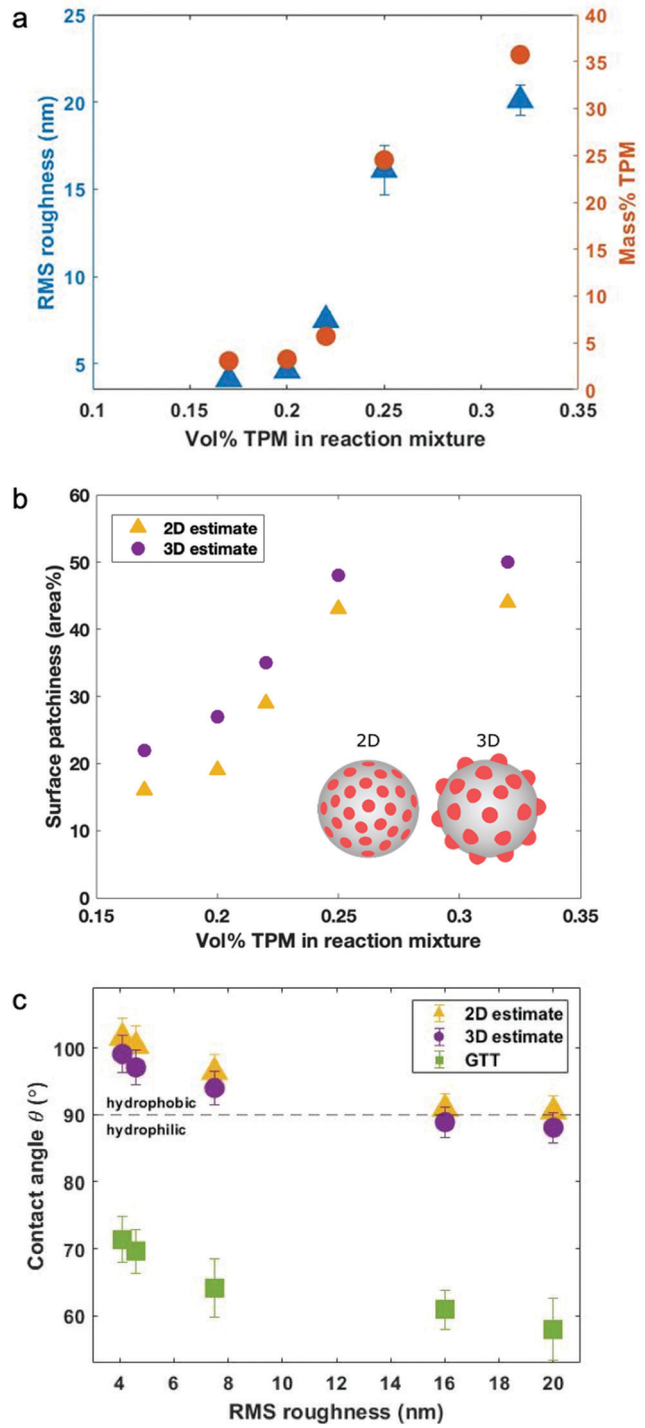

Fig. 3 Particle characterization. (a) Particle characterization by their RMS roughness as determined with AFM and mass% TPM calculated with thermogravimetric analysis (residual particle masses after degradation upon calcination) both as a function of vol% TPM in the reaction mixture. (b) 2D and 3D estimates for the surface patchiness of particles of different compositions. Inset: Schematic representation of the definition of 2D and 3D surface patchiness. (c) Estimated (from surface patchiness) and measured (using the GTT) contact angles of patchy rough particles.

effect of surface morphology on surface roughness is presented elsewhere.[27]

To further characterize the chemical heterogeneous nature of the particles, their surface patchiness was estimated using SEM images. The surface patchiness is defined as depicted in Fig. 3b. The ratio between the red area and the total area (grey + red) numerically quantifies the surface patchiness. The area of the asperities can be estimated in two ways. The 2D and the 3D estimation approximate the asperities as their projected area and as spherical caps, respectively. The results of the estimates are presented in Fig. 3b. As expected, the values of 3D surface patchiness exceed those of the 2D patchiness because the area of the spherical caps is larger than their projected area. Since, in practice, the asperities have a curvature, the 3D estimation matches more closely the reality. Interestingly, the 2D estimation captures the chemical partition of the particle surface irrespective of the roughness. Similar to Fig. 3a, the trend of surface patchiness with vol% TPM has a sigmoidal shape. Effectively, the roughness, composition and surface patchiness all depend in the same manner on the vol% TPM initially added in the reaction mixture.

From the surface patchiness estimations, it is possible to calculate the theoretical contact angles (θ_{theory}) for the rough patchy particles (eqn (2)). For this, the contact angles of the bear TPM and PS spheres were measured using the GTT. The contact angle of the sulfate PS spheres was determined to be 108 ± 7°, which is in good agreement with the contact angles between 101° and 116° reported in the literature.[58,64] This means that PS particles are hydrophobic in nature and therefore protruding in the oil phase. Conversely, the contact angle of TPM is 68 ± 7°, which means that it is hydrophilic. Effectively, the patchy rough colloids proposed in this work are composite particles having dual wettability on the same surface. The contact angles θ for the patchy rough particles were estimated by evaluating Cassie's law[65] for the wetting of heterogeneous surfaces:

$$\cos\theta_{theory} = \sigma_{PS}\cos\theta_{PS} + \sigma_{TPM}\cos\theta_{TPM} \quad (2)$$

with σ_{PS} and σ_{TPM} being the surface area fractions of PS and TPM and θ_{PS} and θ_{TPM} being their contact angles measured using the GTT, respectively. The estimated contact angles are shown in Fig. 3c (yellow triangles and purple circles). In eqn (2), the particles are assumed to be in equilibrium and the kinetic effects are neglected.

The contact angles of the patchy rough colloids were measured using the GTT (Fig. 3c, green squares). Remarkably, the measured contact angles are much lower than the estimated wettability values. Effectively, the particles are more hydrophilic than expected purely from their chemical composition. This further corroborates previous observations indicating that the contact line pinning on the roughness features arrests the adsorption.[26] Contact line pinning can also occur by a sufficiently strong wetting contrast on a single particle surface.[66] Patchy rough particles combine these properties and are expected to alter the onset of phase inversion when used as Pickering stabilizers.

Emulsification and phase inversion

To investigate the effect of the particle heterogeneity on the emulsification, formulation and phase inversion of Pickering emulsions, emulsification experiments with particles having

Open Access Article. Published on 18 July 2020. Downloaded on 4/5/2026 3:19:30 AM.
This article is licensed under a Creative Commons Attribution-NonCommercial 3.0 Unported Licence.

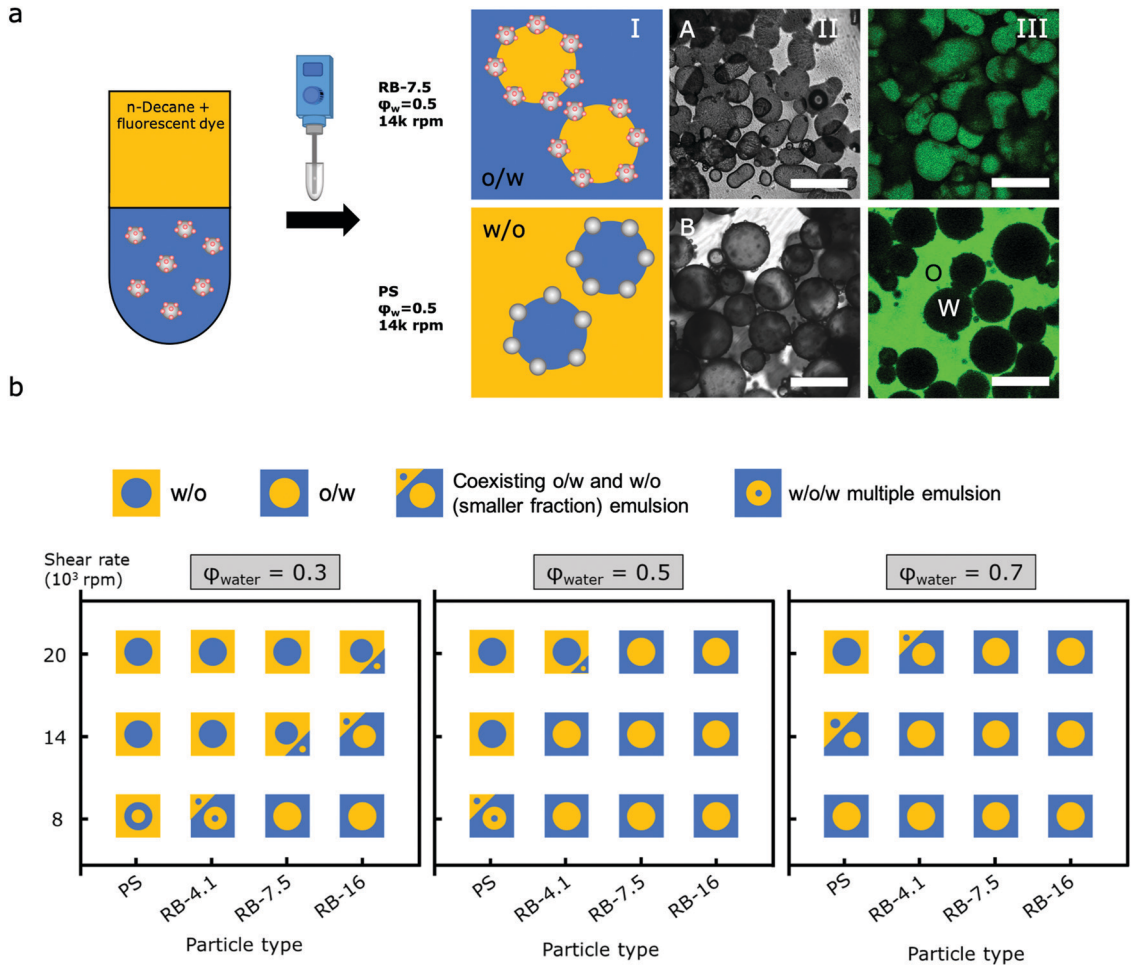

Fig. 4 Emulsification of patchy rough particles. (a-I) Formulation of emulsions and processing parameters varied to obtain either the o/w or w/o emulsion type. (a-II–III) Representative images of o/w (the top row) and w/o (the bottom row) emulsions. (a-II) Bright field microscopy images. (a-III) Confocal fluorescence microscopy images unambiguously reveal the emulsion type upon the addition of BODIPY493/503 in the oil phase. Scale bars: 400 μm. (b) Results of emulsion phase inversion experiments for varying shear rate, φ_{water} and particle type.

different degrees of patchiness were carried out. In particular, the influence of the shear rate, o/w ratio and patchiness on the obtained emulsion type was studied (Fig. 4a-I).

The emulsions were characterized by bright field optical microscopy and confocal fluorescence microscopy (Fig. 4a-II and -III, respectively). The presence of the green fluorescent dye BODIPY in *n*-decane enabled the straight identification of the emulsion type (o/w or w/o, Fig. 4a-III). It should be noted that fluorescent dyes can be surface active and affect emulsions.[67] Therefore, the influence of BODIPY on the water–decane interfacial tensions and on the emulsification was evaluated (see Section S8, ESI†). Even though we concluded that in the selected range of concentrations BODIPY does not affect the emulsification, the emulsions were prepared with the lowest possible concentration of BODIPY to minimize any unexpected interference with the emulsification. Due to the presence of a fluorescent dye as a possible source of impurities, *n*-decane has been used as received. Blank emulsification experiments (without any colloidal stabilizers) reported in Section S8 (ESI†) confirm that all possible impurities contained in *n*-decane during the emulsification experiments do not affect the system.

According to the Bancroft rule, the phase wherein particles can be stably dispersed constitutes the continuous phase of the emulsion. Therefore, the inverted emulsions are of the anti-Bancroft type. Interestingly, in this work all particles form a stable dispersion in aqueous solutions due to charge stabilization, despite the fact that in some cases they are inherently hydrophobic (PS, RB-4.1, RB-7.5). Those colloids can form stable anti-Bancroft type emulsions only if the emulsification conditions allow them to reach their equilibrium position with respect to the interface.

In general, it was observed that rougher particles form with higher success rate emulsion droplets with morphologies that can deviate from circularity compared to smooth particles. This can be clearly observed by comparing Fig. 4a-IIA obtained with RB-7.5 particles with Fig. 4a-IIB generated with PS. This is ascribed to the capillary forces between rough particles trapped at the interface.[68–70] These forces arise from the undulated contact line around the particles, which generates capillary multipoles and consequently a 2D network[71] and imparts deviatory rheological properties to the interface.[72,73] Moreover, for the roughest particles

 This journal is © The Royal Society of Chemistry 2020

Open Access Article. Published on 18 July 2020. Downloaded on 4/5/2026 3:19:30 AM.
This article is licensed under a Creative Commons Attribution-NonCommercial 3.0 Unported Licence.

(RB-20 and also to some extent RB-16), the amount in the dispersed phase was low. This suggests limited adsorption and consequently stabilization capability of the extremely rough and heterogeneous colloids. The observed trend could be due to a transition from Wenzel (for the less rough particles) to Cassie–Baxter (for the roughest particles) wetting. In fact, it has been proposed that, in the latter regime, colloids are less efficient Pickering stabilizers.[74,75] Traces of wetting transitions could not be observed experimentally due to the limited resolution of the used SEM. Additionally, emulsions fabricated with particles having an extreme degree of patchiness presented a higher degree of droplet aggregation. This suggests that very heterogeneous colloids form particle bridging more efficiently. This is very likely connected to the peculiar position that they occupy at liquid interfaces. In fact, their contact angle approaches $\sim 60^\circ$ and this configuration coincides with the wetting ranges for which the probability of particle bridge formation is enhanced.[76] Despite being less pronounced, the tendency to form droplet aggregates has been observed for all other patchy rough particles. This is the reason behind the fact that the meniscus between the emulsion layer and the excess continuous phase is not necessarily straight (see Section S11, ESI†). More details and investigation of the emulsification challenges encountered with the roughest particles are reported in Section S9 (ESI†). Because of its limited emulsification, RB-20 was excluded from the phase inversion experiments.

For PS, RB-4.1, RB-7.5 and RB-16, the volume fraction of the water phase φ_{water} and the shear rate during emulsification were systematically varied (see Fig. 4b). The optical characterization that proves the emulsion types for all the produced emulsions is found in Section S11 (ESI†). When the coexistence of w/o and o/w emulsions was observed, the volume ratio between the emulsion types was estimated by the visual inspection of confocal microscopy images. In this way, the dominating emulsion type could be identified. Two major trends can be observed in Fig. 4b. Firstly, it is possible to appreciate the effect of the shear rate on the emulsion type. Hereafter, we focus our analysis and explanation on $\varphi_{water} = 0.5$. The same reasoning can be applied to $\varphi_{water} = 0.3$ and $\varphi_{water} = 0.7$. It can be noticed that the probability of emulsion inversion, in our case from o/w to w/o, is enhanced with increasing the shear rates, *i.e.* increasing the energy input during emulsification. This phenomenon was already described for rough but chemically homogeneous silica and PS particles in emulsions with $\varphi_{water} = 0.5$.[30] Such mechanical phase inversion is ascribed to the arrested adsorption of particles at the interface due to contact line pinning on asperities. When a rough (mildly) hydrophobic particle is initially dispersed in water, it can form o/w emulsions at low energy input, because the energy barrier that has to be overcome to reach its equilibrium position is not matched. Conversely, higher shear rates can provide enough energy for the relaxation of the contact line over the kinetic barriers (chemical and/or physical), and a w/o emulsion is formed. The same line of thinking is observed for RB-4.1 at $\varphi_{water} = 0.5$ (emulsified from the water). The fact that these particles primarily form o/w emulsions correlates with the contact angle of 71° found using the GTT. The preferred emulsion type would however be w/o as dictated by their surface chemistry according to the contact angle estimated from the surface patchiness calculation. As expected, the emulsion inverts to w/o at higher energy input.

Interestingly, RB-7.5 and RB-16 only form o/w emulsions irrespective of the shear rate for emulsions with $\varphi_{water} = 0.5$. For RB-7.5, the contact angle estimated from their surface chemistry is $>90^\circ$. In this case, the energy barrier due to contact line pinning on surface heterogeneities and asperities is too high to be overcome with the emulsification input. Analogous reasoning applies to RB-16 particles. Additionally, the estimated contact angle of RB-16 is very close to neutral wettability (88.9°). This excludes the possibility to undergo mechanically-induced phase inversion for $\varphi_{water} = 0.5$. Remarkably, mechanical phase inversion is observed for PS, despite the fact that they are smooth particles and allegedly homogeneous. A kinetic barrier to particle adsorption for PS was already observed.[77] It has been observed that the relaxation time at liquid interfaces follows a logarithmic dynamic analogous to creep processes reported for glassy systems. Those timescales are markedly slower than those that would be expected from a mere viscous dissipation process.[78,79] It has been suggested that this non-ideal behavior can be connected to grafted polymer 'hairs' inducing contact line pinning.[80] The latter can explain the observed mechanical phase inversion of PS-stabilized emulsions. For the sake of completeness, TPM-stabilized emulsions have been produced and are shown in Section S10 (ESI†). TPM forms preferentially o/w emulsions in accordance with its hydrophilicity expressed in the measured contact angle of 68°. Surprisingly, for all the conditions probed here phase inversion cannot be reached. This suggests that the anchoring of TPM particles at water–oil interfaces is particularly strong. The unexpectedly high adsorption energy can be associated to the short and violent polymerization strategy that likely forms short (higher probability for recombination) and therefore less entangled polymeric chains, which are more prone to loosening when in contact with liquid interfaces. Those particles may therefore mimic the behavior of core–shell colloids when exposed to liquid interfaces, which are known to possess an exquisite adsorption energy.[81,82]

Secondly, the effect of the overall surface heterogeneity on the phase inversion is displayed in Fig. 4b along the abscissa. For particles with a chemically homogeneous surface, the water volume fraction at which the catastrophic phase inversion occurs depends on the particle wettability.[15,83] At the same time, phase inversion (transitional) from o/w to w/o of emulsions with $\varphi_{water} = 0.5$ can be induced by the addition of hydrophobic colloids to an emulsion initially stabilized only by hydrophilic particles and *vice versa*.[34] Therefor, it can be inferred that the emulsion type is determined by the average wettability of all particles present. Accordingly, in the case of composite particles having dual wettability on the same surface, it is reasonable to conclude that the average wettability of the single particles determines the preferred emulsion type. In particular, as a function of the particle type, the onset of the catastrophic phase inversion is shifted to lower φ_{water} or even suppressed. At a shear rate of 20 000 rpm, the reference colloids with the lowest degree of

Open Access Article. Published on 18 July 2020. Downloaded on 4/5/2026 3:19:30 AM.
This article is licensed under a Creative Commons Attribution-NonCommercial 3.0 Unported Licence.

surface patchiness (PS) can form w/o emulsions at all volume ratios probed. At the same input energy, emulsions stabilized with RB-4.1 switch at φ_{water} = 0.3 and φ_{water} = 0.5, while catastrophic phase inversion is almost completely prevented at φ_{water} = 0.7. This trend is confirmed at a greater degree of surface patchiness. Emulsions with RB-7.5 and RB-16 only undergo phase inversion for φ_{water} = 0.3. From a purely thermodynamic perspective, phase inversion should take place immediately beyond the critical value of φ_{water} = 0.5.[84] Interestingly, this careful analysis neglects dynamic effects in the particle adsorption, which are supposed to cause the deviation of the inversion point from the thermodynamic critical value of φ_{water} = 0.5.[84] The presence of significant surface patchiness and therefore contact line pinning greatly affects the dynamics of particle adsorption introducing kinetic contributions in the equation. A full theoretical elaboration goes beyond the purpose of this work. Interestingly, we observe the formation of multiple emulsions, especially in correspondence with the phase inversion as already reported in the literature.[85,86] The catastrophic phase inversion of emulsions expressed as a function of the particle type is carefully described in Section S10 (ESI†).

Even more notably, the degree of surface patchiness shifts both mechanical and catastrophic phase inversion. The onset of mechanically-induced phase inversion is highly dependent on the height of the kinetic barrier to the equilibrium adsorption. As a consequence, the variation in surface heterogeneity-induced pinning sites among the colloids results in different input energies required to phase-invert the emulsions. In fact, o/w emulsions are more favored for higher degrees of patchiness. The wetting contrast between the PS core (hydrophobic) and the TPM asperities (hydrophilic) exacerbates this behavior.

Thus, the systematic variations of the shear rate, o/w ratio and particle type reveal the importance of particle heterogeneity on the formulation and formation of emulsions.

Conclusions

Heterogeneous patchy rough colloids composed of PS cores decorated with organosilicate asperities have been fabricated with tunable surface roughness and composition. The proposed wet chemical process is reliable and ensures the production of large amounts of monodisperse rough colloidal composites having dual wettability on the same surface and controlled patchiness degree. The latter is achieved by solely tuning the amount of organosilicate (TPM) in the reaction mixture at selected pH and nuclei concentration. In this fashion, patchy rough particles with the root-mean-square surface roughness ranging between 4.1 and 20 nm and compositions of 3.1 to 36 mass% of TPM were obtained. In the system presented in this work, the roughness and chemical nature of the surface are coupled. The roughness of the particles was characterized by scanning individual colloidal particles with AFM. An estimate of their composition expressed in mass% of TPM could be obtained from thermogravimetric analysis. The SEM image analysis allowed for an estimation of the surface patchiness of the particles. The comparison of the estimated contact angles with the empirical contact angles measured *via* the GTT indicates that the adsorption of patchy rough colloids at liquid interfaces can be arrested in metastable positions by contact line pinning at heterogeneity sites (topographical defects, chemical heterogeneities on TPM and PS surfaces, interfaces between TPM and PS). Interestingly, the fabricated patchy rough particles can be used as Pickering emulsifiers of water/*n*-decane systems. Systematic variations in the emulsification shear rate, o/w ratio and particle type corroborate the influence of the particle heterogeneity on the formation and formulation of emulsions. It has been confirmed that mechanically-induced phase inversion of the emulsions can be achieved by colloidal particles presenting a kinetically arrested adsorption pathway. Additionally, a tentative link to the role that kinetic effects at a single particle level have on the phase inversion of Pickering emulsions has been proposed.

The output of the work correlates the surface nature of colloidal particles to the onset of both mechanically-induced and catastrophic phase inversion and opens a future and fruitful scenario for the use of non-ideal colloidal systems in on-demand mechanically switchable emulsions.

Author Contributions

M. Z. and W. K. K. designed the research. M. Z. and H. M. H. W. performed the experimental work. M. Z., H. M. H. W. and W. K. K. wrote the manuscript.

Conflicts of interest

There are no conflicts to declare.

Acknowledgements

M. Z. acknowledges the Swiss National Science Foundation (SNSF) for the financial support through the Early post-doc mobility grant P2EZP2-178502. F. Dekker and L. C. Post are acknowledged for their help with SEM and AFM, respectively.

References

1 E. Dickinson, *Curr. Opin. Colloid Interface Sci.*, 2010, **15**, 40–49.
2 M. N. Yukuyama, D. D. M. Ghisleni, T. J. A. Pinto and N. A. Bou-Chacra, *Int. J. Cosmet. Sci.*, 2016, **38**, 13–24.
3 T. Mizutani, K. Arai, M. Miyamoto and Y. Kimura, *Prog. Org. Coat.*, 2006, **55**, 276–283.
4 Z. Li, M. Xiao, J. Wang and T. Ngai, *Macromol. Rapid Commun.*, 2013, **34**, 169–174.
5 Y. Yang, Z. Fang, X. Chen, W. Zhang, Y. Xie, Y. Chen, Z. Liu and W. Yuan, *Front. Pharmacol.*, 2017, **8**, 287.
6 A. Perazzo, V. Preziosi and S. Guido, *Adv. Colloid Interface Sci.*, 2015, **222**, 581–599.
7 C. Linke and S. Drusch, *Crit. Rev. Food Sci. Nutr.*, 2018, **58**, 1971–1985.

 This journal is © The Royal Society of Chemistry 2020

Open Access Article. Published on 18 July 2020. Downloaded on 4/5/2026 3:19:30 AM.
This article is licensed under a Creative Commons Attribution-NonCommercial 3.0 Unported Licence.

8 B. P. Binks, *Curr. Opin. Colloid Interface Sci.*, 2002, **7**, 21–41.
9 W. Ramsden, *Proc. R. Soc. London*, 1904, **72**, 156–164.
10 S. U. Pickering, *J. Chem. Soc., Trans.*, 1907, **91**, 2001–2021.
11 V. Calabrese, J. C. Courtenay, K. J. Edler and J. L. Scott, *Curr. Opin. Green Sustainable Chem.*, 2018, **12**, 83–90.
12 F. Bouchama, G. A. van Aken, A. J. E. Autin and G. J. M. Koper, *Colloids Surf., A*, 2003, **231**, 11–17.
13 I. Mira, N. Zambrano, E. Tyrode, L. Márquez, A. A. Peña, A. Pizzino and J.-L. Salager, *Ind. Eng. Chem. Res.*, 2003, **42**, 57–61.
14 B. P. Binks and J. A. Rodrigues, *Angew. Chem., Int. Ed.*, 2005, **44**, 441–444.
15 B. P. Binks and P. D. I. Fletcher, *Langmuir*, 2001, **17**, 4708–4710.
16 T. Y. Jeon and J. S. Hong, *Colloid Polym. Sci.*, 2014, **292**, 2939–2947.
17 S. Guillot, F. Bergaya, C. de Azevedo, F. Warmont and J. F. Tranchant, *J. Colloid Interface Sci.*, 2009, **333**, 563–569.
18 J. Du and R. K. O'reilly, *Chem. Soc. Rev.*, 2011, **40**, 2402–2416.
19 A. Yusoff and B. S. Murray, *Food Hydrocolloids*, 2011, **25**, 42–55.
20 D. J. McClements and S. M. Jafari, *Adv. Colloid Interface Sci.*, 2018, **251**, 55–79.
21 S. Jiang, Q. Chen, M. Tripathy, E. Luijten, K. S. Schweizer and S. Granick, *Adv. Mater.*, 2010, **22**, 1060–1071.
22 X. Ji, Q. Zhang, F. Liang, Q. Chen, X. Qu, C. Zhang, Q. Wang, J. Li, X. Song and Z. Yang, *Chem. Commun.*, 2014, **50**, 5706–5709.
23 A. F. Mejia, A. Diaz, S. Pullela, Y.-W. Chang, M. Simonetty, C. Carpenter, J. D. Batteas, M. S. Mannan, A. Clearfield and Z. Cheng, *Soft Matter*, 2012, **8**, 10245.
24 B. Madivala, S. Vandebril, J. Fransaer and J. Vermant, *Soft Matter*, 2009, **5**, 1717–1727.
25 D. Wu, J. W. Chew and A. Honciuc, *Langmuir*, 2016, **32**, 6376–6386.
26 M. Zanini, C. Marschelke, S. E. Anachkov, E. Marini, A. Synytska and L. Isa, *Nat. Commun.*, 2017, **8**, 1–9.
27 M. Zanini, C. P. Hsu, T. Magrini, E. Marini and L. Isa, *Colloids Surf., A*, 2017, **532**, 116–124.
28 Y. Lan, J. Liu, E. Eiser and O. A. Scherman, *Polym. Chem.*, 2019, **10**, 3772–3777.
29 L. C. Bradley, W. Chen, K. J. Stebe and D. Lee, *Curr. Opin. Colloid Interface Sci.*, 2017, **30**, 25–33.
30 M. Zanini, A. Cingolani, C.-P. Hsu, M. Á. Fernández-Rodríguez, G. Soligno, A. Beltzung, S. Caimi, D. Mitrano, G. Storti and L. Isa, *Soft Matter*, 2019, **15**, 7888.
31 Y. Nonomura, N. Kobayashi and N. Nakagawa, *Langmuir*, 2011, **27**, 4557–4562.
32 Y. Lan, J. Choi, H. Li, Y. Jia, R. Huang, K. J. Stebe and D. Lee, *Ind. Eng. Chem. Res.*, 2019, **58**, 20961–20968.
33 B. P. Binks and S. O. Lumsdon, *Langmuir*, 2000, **16**, 2539–2547.
34 B. P. Binks and S. O. Lumsdon, *Langmuir*, 2000, **16**, 3748–3756.
35 B. P. Binks, R. Murakami, S. P. Armes and S. Fujii, *Angew. Chem., Int. Ed.*, 2005, **44**, 4795–4798.
36 B. P. Binks and J. A. Rodrigues, *Angew. Chem., Int. Ed.*, 2007, **46**, 5389–5392.
37 B. P. Binks, L. Isa and A. T. Tyowua, *Langmuir*, 2013, **29**, 4923–4927.
38 E. S. Read, S. Fujii, J. I. Amalvy, D. P. Randall and S. P. Armes, *Langmuir*, 2004, **20**, 7422–7429.
39 S. Fujii, D. P. Randall and S. P. Armes, *Langmuir*, 2004, **20**, 11329–11335.
40 G. Sun, Z. Li and T. Ngai, *Angew. Chem., Int. Ed.*, 2010, **122**, 2209–2212.
41 E. M. Herzig, K. A. White, A. B. Schofield, W. C. K. Poon and P. S. Clegg, *Nat. Mater.*, 2007, **6**, 966–971.
42 K. A. White, A. B. Schofield, P. Wormald, J. W. Tavacoli, B. P. Binks and P. S. Clegg, *J. Colloid Interface Sci.*, 2011, **359**, 126–135.
43 B. P. Binks and S. O. Lumsdon, *Phys. Chem. Chem. Phys.*, 2000, **2**, 2959–2967.
44 P. M. Spiecker, K. L. Gawrys, C. B. Trail and P. K. Kilpatrick, *Colloids Surf., A*, 2003, **220**, 9–27.
45 T. N. Hunter, R. J. Pugh, G. V. Franks and G. J. Jameson, *Adv. Colloid Interface Sci.*, 2008, **137**, 57–81.
46 E. Widerström and R. Öhman, *Master's thesis*, Lund University, 2017.
47 C. Whitby and E. Wanless, *Materials*, 2016, **9**, 626.
48 S. Sacanna, M. Korpics, K. Rodriguez, L. Colón-Meléndez, S. H. Kim, D. J. Pine and G. R. Yi, *Nat. Commun.*, 2013, **4**, 2–7.
49 C. Kang and A. Honciuc, *ACS Nano*, 2018, **12**, 3741–3750.
50 C. Kang and A. Honciuc, *J. Phys. Chem. Lett.*, 2018, **9**, 1415–1421.
51 F. Zhang, L. Cao and W. Yang, *Macromol. Chem. Phys.*, 2010, **211**, 744–751.
52 S. Kawaguchi and K. Ito, *Adv. Polym. Sci.*, 2005, **175**, 299–328.
53 Y. Liu, K. V. Edmond, A. Curran, C. Bryant, B. Peng, D. G. A. L. Aarts, S. Sacanna and R. P. A. Dullens, *Adv. Mater.*, 2016, **28**, 8001–8006.
54 C. van der Wel, R. K. Bhan, R. W. Verweij, H. C. Frijters, Z. Gong, A. D. Hollingsworth, S. Sacanna and D. J. Kraft, *Langmuir*, 2017, **33**, 8174–8180.
55 W. Reusch, Free Radical Polymerization, https://chem.libretexts.org/LibreTexts/Purdue/Purdue_Chem_26100%3A_Organic_Chemistry_I_(Wenthold)/Chapter_08%3A_Reactions_of_Alkenes/8.7.%09Polymerization/Free_Radical_Polymerization, accessed 26 September 2018.
56 N. D. Denkov, O. D. Velev, P. A. Kralchevsky, I. B. Ivanov, H. Yoshimura and K. Nagayama, *Langmuir*, 1992, **8**, 3183–3190.
57 B. Bhushan, *Modern Tribology Handbook: Volume One: Principles of Tribology*, CRC Press LLC, 2001, pp. 49–119.
58 V. N. Paunov, *Langmuir*, 2003, **19**, 7970–7976.
59 A. D. Nikolov, D. T. Wasan, A. Chengara, K. Koczo, G. A. Policello and I. Kolossvary, *Adv. Colloid Interface Sci.*, 2002, **96**, 325–338.
60 O. J. Cayre and V. N. Paunov, *Langmuir*, 2004, **20**, 9594–9599.
61 B. P. Binks, B. Duncumb and R. Murakami, *Langmuir*, 2007, **23**, 9143–9146.
62 T. F. Tadros, *Colloid Stability*, Wiley-VCH Verlag GmbH & Co. KGaA, Weinheim, 2007.

Open Access Article. Published on 18 July 2020. Downloaded on 4/5/2026 3:19:30 AM.
This article is licensed under a Creative Commons Attribution-NonCommercial 3.0 Unported Licence.

63 X. Zhang, Y. Sun, Y. Mao, K. Chen, Z. Cao and D. Qi, *RSC Adv.*, 2018, **8**, 3910–3918.
64 A. Maestro, E. Guzmán, F. Ortega and R. G. Rubio, *Curr. Opin. Colloid Interface Sci.*, 2014, **19**, 355–367.
65 A. B. D. Cassie, *Discuss. Faraday Soc.*, 1948, **3**, 11–16.
66 P. G. De Gennes, *Rev. Mod. Phys.*, 1985, **57**, 827–863.
67 J. H. J. Thijssen, A. B. Schofield and P. S. Clegg, *Soft Matter*, 2011, **7**, 7965.
68 B. Madivala, J. Fransaer and J. Vermant, *Langmuir*, 2009, **25**, 2718–2728.
69 R. van Hooghten, L. Imperiali, V. Boeckx, R. Sharma and J. Vermant, *Soft Matter*, 2013, **9**, 10791–10798.
70 P. J. Beltramo, M. Gupta, A. Alicke, I. Liascukiene, D. Z. Gunes, C. N. Baroud and J. Vermant, *Proc. Natl. Acad. Sci. U. S. A.*, 2017, **114**, 10373–10378.
71 J.-B. Fournier and P. Galatola, *Phys. Rev. E: Stat., Nonlinear, Soft Matter Phys.*, 2002, **65**, 031601.
72 K. D. Danov and P. A. Kralchevsky, *Adv. Colloid Interface Sci.*, 2010, **154**, 91–103.
73 E. Vignati and R. Piazza, *Langmuir*, 2003, **19**, 6650–6656.
74 A. San-Miguel and S. H. Behrens, *Langmuir*, 2012, **28**, 12038–12043.
75 C. J. Mable, N. J. Warren, K. L. Thompson, O. O. Mykhaylyk and S. P. Armes, *Chem. Sci.*, 2015, **6**, 6179–6188.
76 D. J. French, P. Taylor, J. Fowler and P. S. Clegg, *J. Colloid Interface Sci.*, 2015, **441**, 30–38.
77 D. M. Kaz, R. McGorty, M. Mani, M. P. Brenner and V. N. Manoharan, *Nat. Mater.*, 2012, **11**, 138–142.
78 C. E. Colosqui, J. F. Morris and J. Koplik, *Phys. Rev. Lett.*, 2013, **111**, 028302.
79 A. M. Rahmani, A. Wang, V. N. Manoharan and C. E. Colosqui, *Soft Matter*, 2016, **12**, 6365–6372.
80 A. Wang, R. McGorty, D. M. Kaz and V. N. Manoharan, *Soft Matter*, 2016, **12**, 8958–8967.
81 S. A. Vasudevan, A. Rauh, L. Barbera, M. Karg and L. Isa, *Langmuir*, 2018, **34**, 886–895.
82 S. A. Vasudevan, A. Rauh, M. Kröger, M. Karg and L. Isa, *Langmuir*, 2018, **34**, 15370–15382.
83 B. P. Binks and S. O. Lumsdon, *Langmuir*, 2000, **16**, 8622–8631.
84 P. A. Kralchevsky, I. B. Ivanov, K. P. Ananthapadmanabhan and A. Lips, *Langmuir*, 2005, **21**, 50–63.
85 B. P. Binks and J. A. Rodrigues, *Langmuir*, 2003, **19**, 4905–4912.
86 P. S. Clegg, J. W. Tavacoli and P. J. Wilde, *Soft Matter*, 2016, **12**, 998.

This journal is © The Royal Society of Chemistry 2020